Chapter-4

Ion Dynamics of Non-Stiochiometric $Na_{0.5+x}Bi_{0.5-x}TiO_{3-\delta}$: A Degradation Study

Pragati Singh, *Pardeep K. Jha, A.S.K. Sinha, Priyanka A. Jha, Prabhakar Singh,* ***"****Ion dynamics of non-stoichiometric* $Na_{0.5+x}Bi_{0.5-x}TiO_{3-\delta}$*: A degradation study", Solid State Ionics, 2020, 345,115158.*

CHAPTER 4: Ion Dynamics of Non-Stoichiometric $Na_{0.5+x}Bi_{0.5-x}TiO_{3-\delta}$: A Degradation Study

4.1 Introduction

In chapter 3, it has been studied that how the conduction mechanism in NBT changes with the sintering temperature. Also, the NBT sample degrades in the reducing atmosphere. The non-stoichiometry of Na and Bi in NBT plays a very vital role in the conduction mechanism. The oxygen content affects very badly as both Na and Bi are volatile in nature. The oxide ion conductivity is reported to increase with the enhancement of sodium or bismuth deficient NBT[167][168]. In the case of NBT, conductivity is mainly governed by A-site non-stoichiometry. The first principle calculations also proved enhancement in the conductivity with A/B site acceptor doping[169]. In the case of electrolyte material for SOFC, the conduction is mainly with sublinear frequency dependence related to oxygen ion migration[170].

This chapter presents a comprehensive investigation of the ion dynamics in NBT with the change in A site stoichiometry. For this purpose, $Na_{0.5+x}Bi_{0.5-x}TiO_{3-\delta}$ (x = -0.02, -0.01, 0.00, 0.01, 0.02) have been prepared by solid-state reaction route. In order to understand the degradation of NBT, we have planned to investigate whether the degradation is due to stoichiometry or else. In this regard, the as-prepared sample was studied in detail both before and after reduction.

4.2 Experimental Procedure

$Na_{0.5+x}Bi_{0.5-x}TiO_{3-\delta}$ (x = -0.02, -0.01, 0.00, 0.01, 0.02) solid solutions were prepared using the Solid state reaction route. Na_2CO_3 (Rankem; 99.5%), Bi_2O_3 (Alfa Aesar; 99%), TiO_2 (Alfa Aesar; 99.8%) were used as the carbonates and oxides regent. The details of the sample preparation have been mentioned in chapter 2.

The phase purity of the samples were monitored by X-Ray diffractometer with Cu-Kα radiation (RigakuMiniflex desktop X-ray diffractometer) in the $2\theta \sim 20^{o}$ - 70^{o} at the scan rate of 2^{o}/min. The density measurement was carried out using Archimedes density measurement kit (DENVER SI-234). The sintered samples are observed to be 99% dense. The morphology and compositional analysis were carried out using SEM and EDX (EVO-Scanning electron microscope MA15 / 18). The impedance measurements were carried on platinum coated pellet using (Wayne Kerr LCR meter (6500 P Series) from room temperature to 700^{o}C in the frequency range of 24Hz to 1MHz at the amplitude of 1 V. Thermogravimetric analyses of the sintered powders were done using Metler DSC/TGA system under continuous purging of nitrogen gas. The elemental composition was further verified using X-ray photoelectron spectroscopy (Kratos Amicus model) high performance analytical instrument utilizing Mg target under 10^{-6} Pa pressure.

4.3 Results and Discussion

4.3.1 Structural Studies

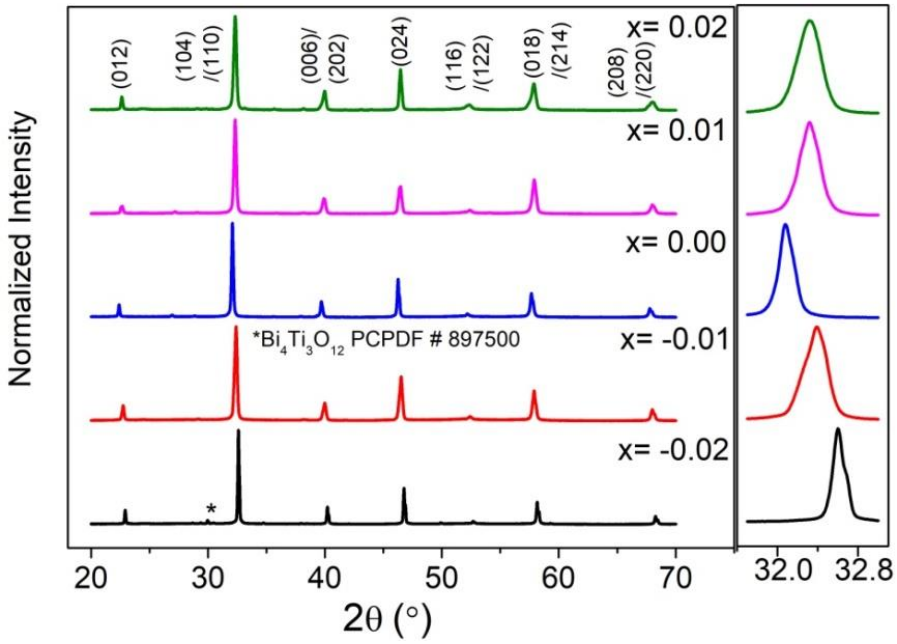

Figure 4.1: X-ray diffractograms of the $Na_{0.5+x}Bi_{0.5-x}TiO_{3-\delta}$ (x = -0.02,-0.01, 0.0, 0.01 and 0.02) compositions

Figure 4.1 shows the nearly single phase X-ray diffractograms of the studied compositions. A secondary phase at $2\theta \approx 30^{o}$ is observed in the XRD pattern of x = - 0.02 sample, and this corresponds to $Bi_4Ti_3O_{12}$ according to PCPDF file No. # 897500. While the phase purity of the compositions studied is > 98%. In addition, with the further increase in Bi content, this secondary phase increases (x = -0.04, graph not shown here). The Rietveld refinement of XRD data is done with R3*c* symmetry using Full Prof Suite package in structural Rietveld mode (Fig. 4.2). After applying zero correction of the instrument, Pseudo - Voigt peak profile is used for refinement. The goodness of square fit (χ^2) obtained after Rietveld

refinement were found to lie within the appreciable range (Table 4.1). The structure of the samples is analysed using Diamond 3.0 software.

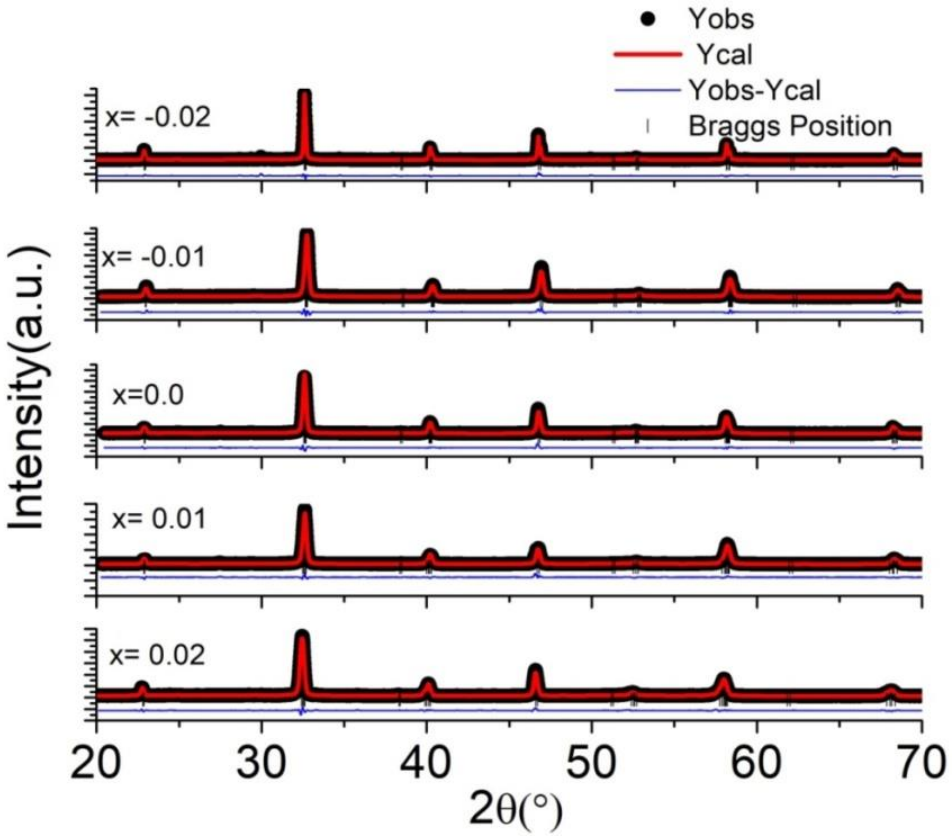

Figure 4.2: Rietveld refined X-ray diffractograms of the studied $Na_{0.5+x}Bi_{0.5-x}TiO_{3-\delta}$ (x = -0.02, -0.01, 0.0, 0.01 and 0.02) compositions

Table 4.1: Lattice Parameters, atomic positions and goodness of fitting parameters of the studied $Na_{0.5+x}Bi_{0.5-x}TiO_{3-\delta}$ (x = -0.02, -0.01, 0.0, 0.01 and 0.02) compositions

Sample x	**Atoms**	**Position**			**R-factor**			**Lattice Parameters (Å)**
		x	y	z	χ^2	Bragg R-factor	R_f factor	
-0.02	Na	0	0	0.255(1)	11.4	3.40	2.93	a = b= 5.488(6) c=13.334(3)
	Bi	0	0	0.255(1)				
	Ti	0	0	0.004(6)				
	O	-0.176(8)	0.336(6)	0.053(4)				
-0.01	Na	0	0	0.257(5)	8.21	3.02	1.57	a= b=5.523(8) c=13.333(5)
	Bi	0	0	0.257(5)				
	Ti	0	0	0.021(2)				
	O	-0.193(5)	0.380(6)	0.081(4)				
0.0	Na	0	0	0.254(4)	6.37	3.00	1.80	a= b=5.573(7) c=13.153(1 0)
	Bi	0	0	0.254(4)				
	Ti	0	0	0.006(6)				
	O	-0.174(4)	0.302(5)	0.060(3)				
0.01	Na	0	0	0.277(1)	12.4	3.43	2.05	a= b=5.537(2) c=13.255(3)
	Bi	0	0	0.277(1)				
	Ti	0	0	0.043(1)				
	O	-0.150(3)	0.353(5)	0.085(9)				
0.02	Na	0	0	0.251(4)	6.99	2.13	1.91	a= b=5.537(6) c=13.020(1)
	Bi	0	0	0.251(4)				
	Ti	0	0	0.000(3)				
	O	-0.189(3)	0.316(5)	0.044(6)				

The volume obtained from the Rietveld refinement of the X-ray diffractograms is plotted in Fig. 4.3 with the tolerance factor. It is observed that with the increase in Na content, volume decreases and tolerance factor decreases. The structure is becoming more disordered with the increase in volume in Na rich compositions. While in Bi rich regime inverse correlation between tolerance factor and volume is obtained. In addition, the lattice parameter 'a' is observed to decrease with the increase in x in both Na rich and Bi rich compositions. It is in

correlation with the shifting of peak $2\theta \approx 32^{o}$ with the increase in Na and Bi content. It is noticeable that ionic radii of Bi^{3+} (1.03 Å) and Na^{+} (1.02 Å) same but, due to the difference in the mass ($\Delta A \sim 186$) and charge (2) of Bi^{3+} and Na^{+}, diffuseness will vary significantly with increase in the x, as massive Bi^{3+} will reduce in number while light Na^{+} increases. This will not only generate non-stoichiometry also alter the lattice potential[171]. This alteration of lattice variation is dynamic process that will depend upon the thermodynamical state of the sample. In the present case, the alteration in Na^{+}/Bi^{3+} ratio with x is reflected in the lattice parameter variation.

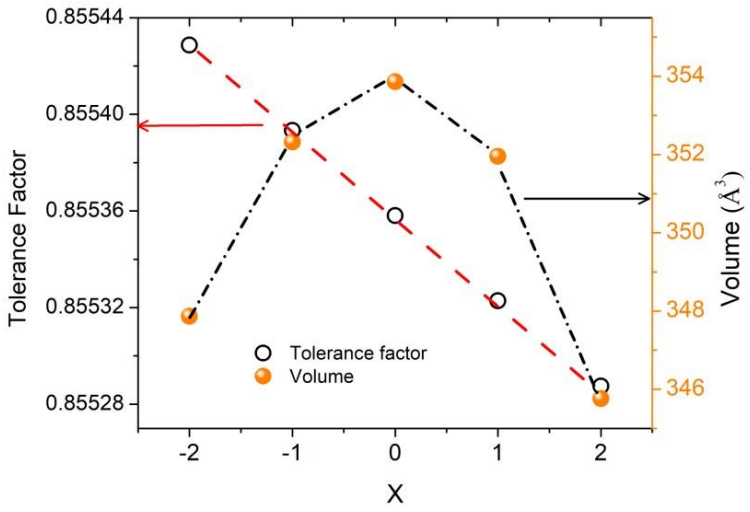

Figure 4.3: Volume and tolerance factor of the studied $Na_{0.50+x}Bi_{0.50-x}TiO_{3-\delta}$ (x = -0.02,-0.01,0.0,0.01 and 0.02) compositions

4.3.2 Microstructural Analysis

Figure 4.4 (a-e) shows the SEM micrographs of the studied $Na_{0.5+x}Bi_{0.5-x}TiO_{3-\delta}$ (x = -0.02, -0.01, 0.0, 0.01 and 0.02) compositions. The polycrystalline nature of microstructure with broad distribution of grain size is observed. The average grain size is calculated using Image J software, and its value is found to increase with the increase in non-stoichiometry and lies

between 1.34 - 20.0μm. The change in the morphology from cube shaped grains (faceted) for x = -0.02 to hexagonal grains (rough) for x = 0.02 is observed. In addition, some secondary phases are visible in x = 0.02 and x = 0.01 sample which we are unable to detect through XRD. It is well known in NBT that most of the times the secondary phases are not visible in XRD[168][172]. Hence, various other techniques are being employed to elucidate the secondary phases. In the current state, the secondary phases are also analysed through XPS and discussed in later section.

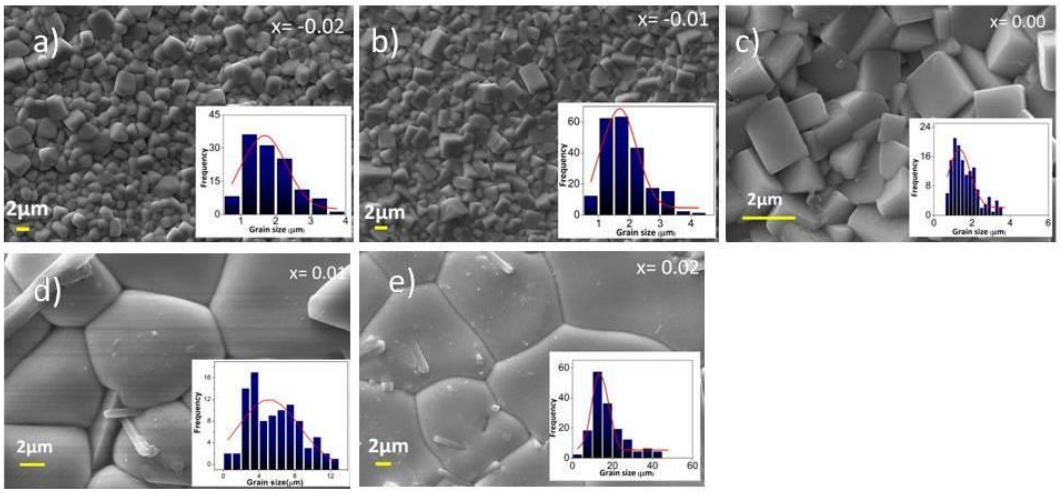

Figure 4.4 (a-e): SEM micrographs of the studied $Na_{0.5+x}Bi_{0.5-x}TiO_{3-\delta}$ (x = -0.02, -0.01, 0.0, 0.01 and 0.02, (a-e)) compositions

4.3.3 X-ray Photoelectron Spectroscopy Analysis

To find out the elemental compositions, we have done X-ray photoelectron spectroscopy measurements of the studied $Na_{0.5+x}Bi_{0.5-x}TiO_{3-\delta}$ (x = -0.02, 0.0, 0.01 and 0.02) compositions. The wide spectrum of the XPS data is analysed using the standard look up table for XPS and is matching well with the standard ones (Fig. 4.5 and 4.6). There is no peak shifting observed for Na and Bi de-convoluted data. The XPS peak of Na lies around 1071eV and is surrounded by TiLLM auger. Hence, Na 1s peak is quantified by de-convoluting the auger peaks. For Bi,

it consists of $4f_{5/2}$ and $4f_{7/2}$ peaks corresponding to metallic Bi and Bi_2O_3. It is observed that the quantity of Bi metal is increasing in comparison to Bi_2O_3 with the increase in x. According to the standard look up table, Ti splits spin-orbit components, and it varies chemical state with energy 6.1 eV. It comprises of $2p_{1/2}$ and $2p_{3/2}$ along with a satellite peak, and Ti $2p_{1/2}$ peak is shorter and short-lived than Ti $2p_{3/2}$ peak. It is also very difficult to de-convolute Ti peaks due to the presence of multiple oxidation states. The red and blue shift observed with x corresponds to the change in oxidation states of Ti and O. This shifting of peaks reveals the electron transfer in between Ti and O. Simultaneously, it is also observed that the intensity of satellite peak is increasing with x showing the occupancy of vacancy by electrons. Also, satellite peak is observed due to metal-ligand interaction, i.e. interaction of p- orbital of O and d-orbital of Ti [173]–[175]. Further, O XPS peaks are de-convoluted, and it consists of oxide, hydroxide and auger peaks. This auger peak is found to be in correlation with the satellite peak observed in Ti showing the occupancy of oxygen vacancy through the electron. This might be due to the Bi-lone pair interaction and also reflects the electron cloud shifting from O-anion. Additionally, significant p-d interaction observed between filled p-orbital and empty d-orbital of Ti is leading to the formation of secondary phases in NBT with the alteration in Na/Bi ratio. As observed in the Na rich and Bi rich compositions, secondary phases are formed at $x = \pm 0.02$, hence discarded from further measurements.

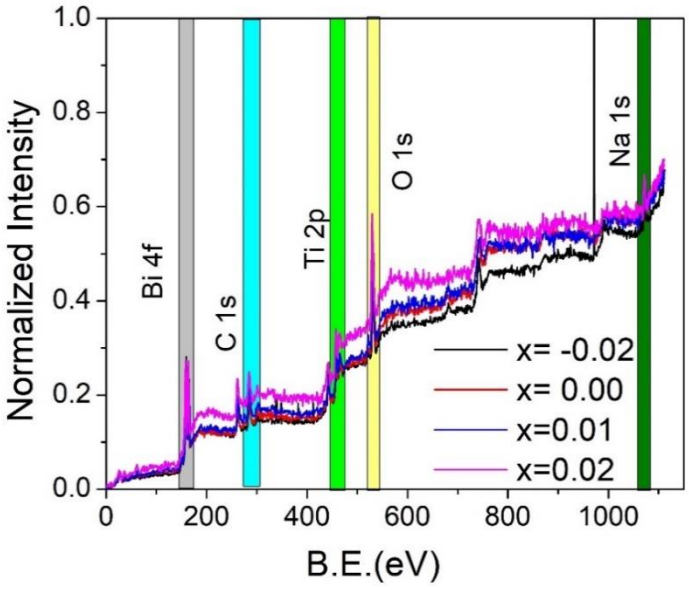

Figure 4.5: Wide range X-Ray photoelectron spectra of $Na_{0.5+x}Bi_{0.5-x}TiO_{3-\delta}$ (x = -0.02, 0.00, 0.01 and 0.02) compositions showing the presence of Na, Bi, Ti and O

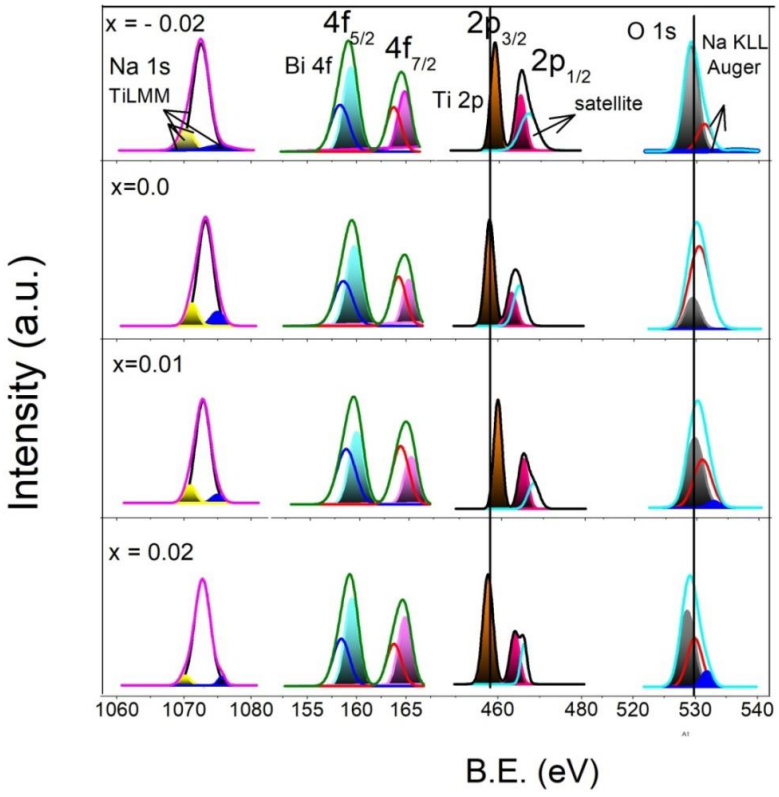

Figure 4.6: X-ray photoelectron spectroscopy measurements (de-convoluted peaks)of the studied $Na_{0.5+x}Bi_{0.5-x}TiO_{3-\delta}$ (x = -0.02, 0.0, 0.01 and 0.02) compositions

Table 4.2: Area of the peaks obtained from XPS peak fitting

Elements		**x = 0.02**	**x = 0.0**	**x = 0.01**	**x = 0.02**
Na	Na 1s	31264.44	22194.38	19098.94	14168.76
	TiLMM	5735.476	2495.408	1171.25	851.7553
	TiLMM	2272.657	3691.789	2583.175	508.378
Bi	Bi $4f_{5/2}$	46351.27	30797.52	20867.86	15495.52
		29038.64	13524.28	12370.94	11866.7
	Bi $4f_{7/2}$	30156.59	20020.71	19833.46	9589.522
		23191.33	17308.94	18108.82	7776.287
Ti	$Ti2p_{3/2}$	27149.54	21499.22	14892.67	13560.6
	$Ti2p_{1/2}$	15644.56	7372.046	4894.498	5911.95
	Satellite	18621.2	10370.07	7891.014	3197.279
O	O1s	82357.76	82622.3	58565.9	61117.58
		20192.23	22132.82	42605.18	38311.6
	Na KLL Auger	1657.01	2142.642	3634.107	9453.296

In addition, O 1s peak at ~ 529 eV is ascribed to the metal and O bond (Na-O, Bi-O and Ti-O) while, 2nd peak of O belongs to the metal-hydroxide bond. The ratio of area of peaks corresponding to metal-oxygen and metal-hydroxide corresponds to the oxygen vacancy concentration. Here, the ratio of area of peaks (see Table 4.2) is observed to decrease with the increase in x and showing the decrease in oxygen vacancy concentration with x. The reduction in oxygen content (δ) has been estimated and verified through Thermogravimetric analysis in the N_2 atmosphere.

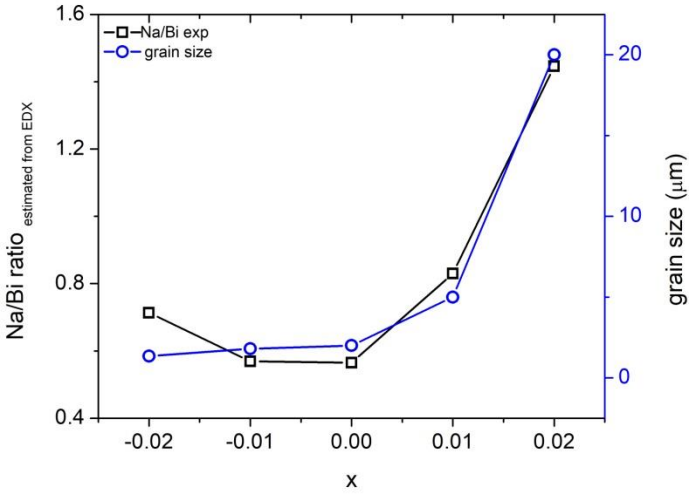

Figure 4.7: Depicts the Na/Bi ratio and grain size obtained from XPS and grain histograms, respectively (lines are a glide to the eye)

It is observed in Fig. 4.7 that Na/Bi ratio obtained from XPS and grain size obtained from grain size histograms are observed to increase with x. In the present case, grain size increases with the increase in Na/Bi ratio[176] and the grain/grain boundary morphology changes from faceted to rough with the increase in x. This change has been well explained by grain boundary roughening[177]. As rough grain boundaries (joined) have smaller driving force for movement of grain boundary leading to the increase in grain size with the increase in Na/Bi content. Hence, with faceted grains, the grain growth is inhibited due to higher driving force[176].

4.3.4 Thermogravimetric Analysis (TGA)

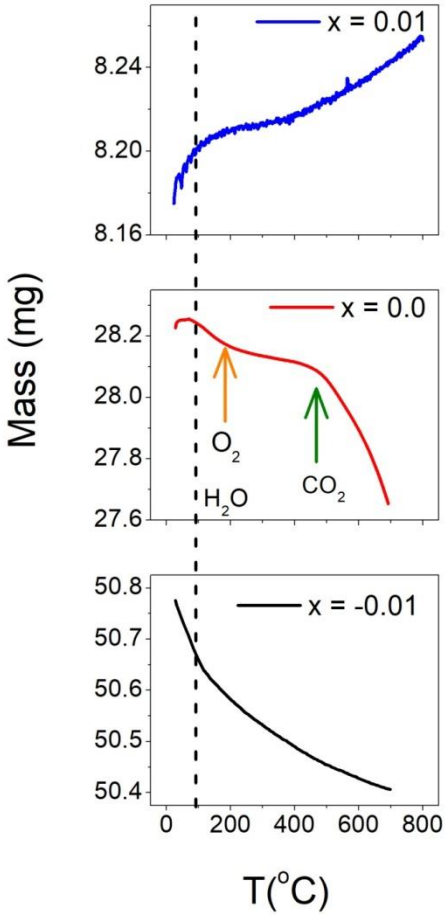

Figure 4.8: Thermogravimetric analysis of the studied $Na_{0.5+x}Bi_{0.5-x}TiO_{3-\delta}$ (x = -0.01, 0.0 and 0.01) compositions

A gradual mass loss is observed for x = -0.01 sample with a kink at nearly 100 ℃ (shown in Fig. 4.8). For x = 0.0 sample, mass loss with three kinks are observed at ~100 ℃, 240 ℃ and 450 ℃. These kinks correspond to the weight loss due to H_2O, O_2 and CO_2 as the weight loss observed are ~ 2%, 3.5% and 4.9%, respectively. Further, δ has been estimated using the following reaction and illustrated in Table 4.3[178]. It is nearly observed in accordance with the estimation of δ from XPS. Further, due to the availability of two volatile materials, EDX data has not been used for the estimation of O and Na content.

$$Na_2CO_3 + Bi_2O_3 + 4TiO_2 \rightarrow 4Na_{0.5}Bi_{0.5}TiO_{3-\delta} + CO_2 + \frac{4}{2}\delta O_2 \uparrow \quad (4.1)$$

Table 4.3: δ obtained from TGA and XPS

Composition	δ obtained from TGA_N_2 atm	δ obtained from XPS
x = -0.02	×	-0.05
x = -0.01	-0.06	×
x = 0.0	-0.04	-0.055
x = 0.01	0.02	0.0
x = 0.02	×	0.01

× Data not available

4.3.5 AC Conductivity Formalism

In order to understand the conduction mechanism with the Na/Bi ratio, variation of the log of conductivity vs log frequency is shown in Fig. 4.9 (a). Figure 4.9 (a) shows the Jonscher power law[148] fitting for x = 0.0 sample. The solid line represents the power line fitted curve, and the symbol represents the experimental data. The experimental and the fitted data are found to be in close agreement with each other. A plateau region corresponding to dc conductivity and the increase in conductivity with the frequency after hopping frequency is observed in the present case. Through Jonscher power law, dc conductivity σ_{dc}, hopping frequency, ν_h and exponent are evaluated[153][166]. At x = -0.01, the value of exponent is greater than 1 and is observed to increase with the increase in temperature up to 600 ℃ and then observed to decrease with the increase in temperature (Fig. 4.9(b)). At x = 0.0, the exponent decreases with the increase in temperature and at x = 0.01, the value of exponent is observed to decrease with temperature up to 600 ℃ and thereafter increases. In addition, for x = 0.0 and 0.01, the value of exponent is less than 1. The decrease in exponent with the increase in temperature is

attributed to the overlapping large hopping polaron tunnelling model due to the formation of oxygen vacancies[179]. The change in exponent behaviour suggests the conversion from super-linear in the Bi rich region with the sub-linear behaviour in Na rich regime. For the confirmation of super-linear behaviour in the exponent, we have plotted log σ_{dc} and log ν_h for the studied compositions (Fig. 4.9 (c)). It is observed in Fig. 4.9 (c) that the slope of log σ_{dc} and log ν_h for x = -0.01 is greater than 1 while for x = 0 and 0.01, it is less than 1. The activation energy estimated using Arrhenius relation $\sigma_{dc}T = \sigma_0 \exp\left(\frac{-E_a}{KT}\right)$, is in the range of 1.4-1.9 eV (Fig. 4.9(d)). It is recently concluded that value of activation energy, E_a, between 2eV and 4 eV is required for the migration of Na^+ ion, for Bi^{3+} it lies between 5 – 9 eV[169]. E_a lies in between 1.82 eV and 0.93 eV for the migration of oxygen ions from NaO^- layer to TiO_2 layer[154][180]. Thus, this activation energy of the range of 1.4 - 1.8 eV suggests the migration of oxygen ions from NaO^- layer to TiO_2 layer. The difference of 0.4 eV is observed in accordance with the change in Na^+/Bi^{3+} ratio. This is possibly due to the different local chemical environments for oxygen ions/vacancies created by the order-disorderness and change in grain size with the variation of Na^+/Bi^{3+}. Normally, the sublinear frequency dependent behaviour occurs due to quantum mechanical tunnelling or classical hopping between the two localized states related with the oxygen ion migration as suggested in the Introduction section. While, it is proposed that in the case of super linear behaviour, there is simultaneous hopping of two electrons over the barrier separating two oppositely charged centres[170]. Hence, in the present case, oxygen vacancies coupled with electrons start to migrate between two localized states in electron-rich Bi dominant compositions in comparison to electron deficient Na rich compositions.

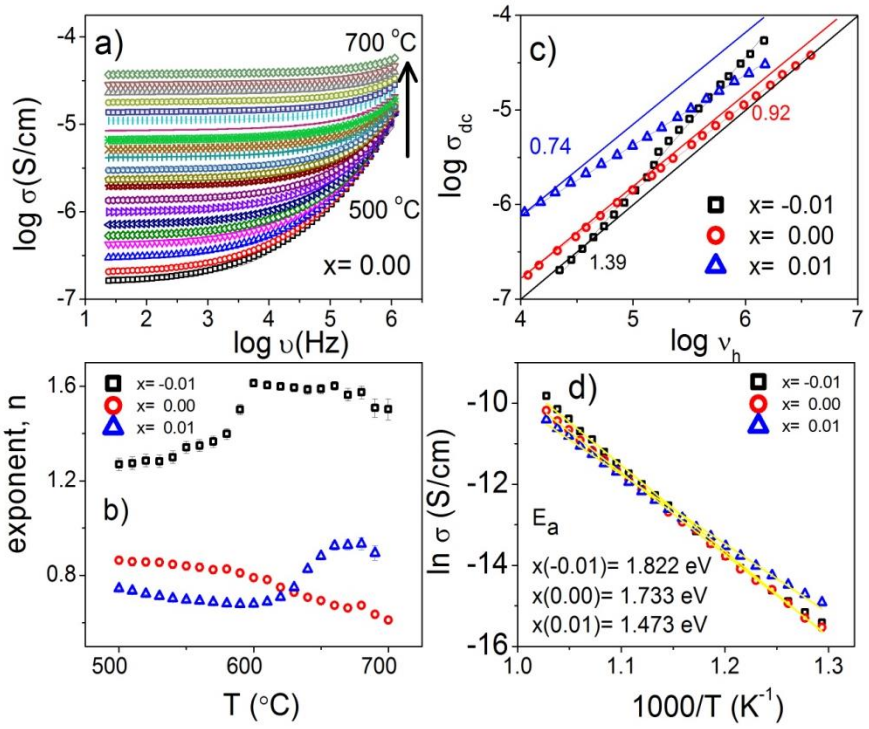

Figure 4.9: (a) Variation of log σ vs log ν for x =0.0 sample (for instance), **(b)** Variation of exponent with temperature, **(c)** Variation of log σ_{dc} vs log ν_h and **(d)** Arrhenius fitting of conductivity

In our earlier paper, we have seen that NBT degraded in reducing atmosphere[181]. Further, to study its degradation behaviour, we have dipped three phase pure samples x = -0.01, 0.0 and 0.01 in propan-2-ol for 48 h and then studied properties. A comparative is studied for the structural and electrical properties before and after reducing.

4.4 Degradation Mechanism

4.4.1 Structural Properties Before and After Reduction

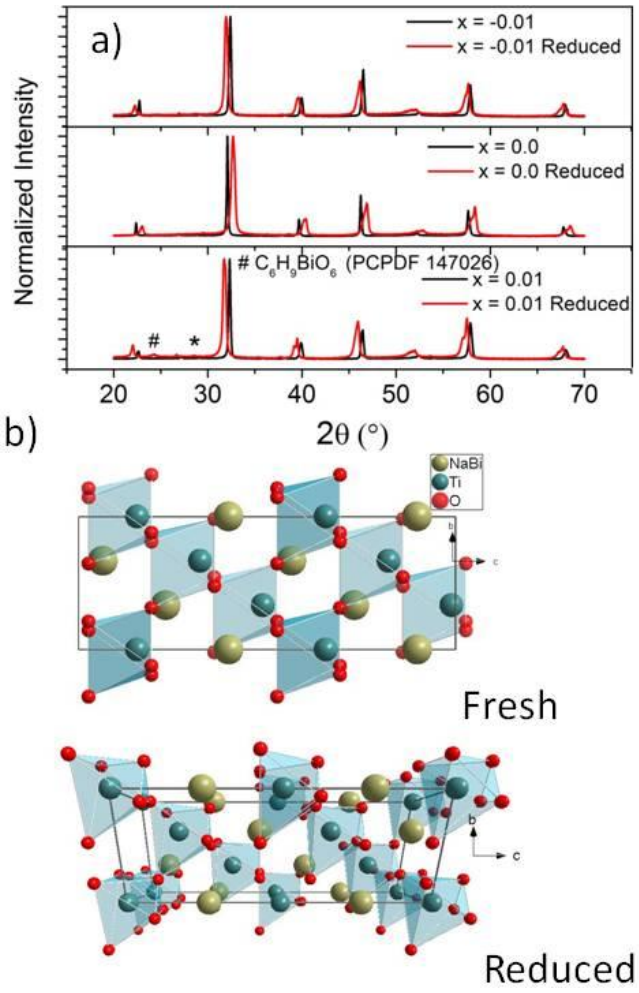

Figure 4.10: (a) Comparative of X-ray diffractograms of the fresh and reduced samples and **(b)** Visualization of unit cell structure of fresh and reduced sample of composition with x = 0.0

Table 4.4: Lattice Parameters, atomic positions and goodness of fitting parameters of the studied $Na_{0.5+x}Bi_{0.5-x}TiO_{3-\delta}$ (x = -0.01, 0.0, 0.01) compositions after reducing

Sample x	Atoms	Position			R-factor			Lattice Parameters (Å)
		x	y	z	χ^2	Bragg R-factor	R_f factor	
-0.01	Na	0	0	0.257(5)	9.03	8.8	9.3	a = b= 5.5151(1)
	Bi	0	0	0.257(5)				c=13.5953(3)
	Ti	0	0	0.004(8)				
	O	-0.157(6)	0.376(3)	0.108(4)				
0.0	Na	0	0	0.2546(5)	6.47	9.89	12.6	a= b=5.4411(4)
	Bi	0	0	0.2546(5)				c=13.2426(17)
	Ti	0	0	0.0066(9)				
	O	-0.161(7)	0.256(2)	0.056(6)				
0.01	Na	0	0	0.2602(7)	9.37	10.10	13.8	a= b=5.5975(1)
	Bi	0	0	0.2602(7)				c=13.594(7)
	Ti	0	0	0.0216(1)				
	O	-0.141(6)	0.236(6)	0.0707(2)				

Table 4.5: Lattice Parameters, atomic positions and goodness of fitting parameters of the sample dipped in propanol for 48h

Sample x	Atoms	Position			R-factor		Lattice Parameters (Å)
		x	y	z	Bragg R-factor	R_f factor	
	Na	0	0	0.25752	16.2	15.0	a= b=5.5145
-0.01	Bi	0	0	0.25752			c=13.6015
	Ti	0	0	0.00448			
	O	-0.15744	0.37635	0.10840			
	Na	0	0	0.25465	6.47	5.90	a= b=5.4410
0.00	Bi	0	0	0.25465			c=13.1230
	Ti	0	0	0.00669			
	O	-0.16171	0.25652	0.05600			
	Na	0	0	0.26027	9.65	7.95	a= b=5.5975
0.01	Bi	0	0	0.26027			c=13.5947
	Ti	0	0	0.02160			
	O	-0.14161	0.23661	0.07072			

Figure 4.10 depicts the comparative of X-ray diffractograms of the fresh and reduced samples. It is observed that at x = 0.0, the XRD peaks shift to the higher angle after reduction

showing lattice contraction. Whereas, in non - stoichiometric samples, i.e., x = 0.01 and x = 0.01, XRD peaks shift to the lower angle side showing lattice expansion. In addition, at x = 0.01, a secondary phase appeared in addition to the secondary phase earlier present in the sample. The secondary phase corresponds to $C_6H_9BiO_6$ (PCPDF No. 147026) with the reaction of NBT with propan-2-ol. The shifting of XRD pattern is further refined through Rietveld refinement using zero correction of the instrument to avoid any errors regarding the shifting of the peaks (see Table 4.4 and 4.5). The goodness of fitting parameters is found to lie within the errors of appreciable range. In addition, the lattice parameter 'c' (13.1530 Å) is observed to decrease after reduction (13.1230 Å). The volume decreases, and density increases after reduction (336.458 $Å^3$, 6.27 gm/cm^3) after reduction. However, the gap of the peak shift is almost similar at lower and higher angles, i.e. 22^o and 68^o, respectively. Regardless of the same gap between the peak positions, it is observed that atomic arrangements corresponding to O have drastically changed, leading to the changes in the structure after reducing atmosphere.

4.4.2 Electrical Properties before and after reduction

Figure 4.11 shows the comparative of logσ vs log ν of the fresh and reduced x = 0.0 sample (for instance). It is observed that in the fresh sample, there is merging of the conductivity isotherms at higher frequency while there is no merging observed at higher frequency in reduced sample. This indicates the change in the hopping rate of charge carriers after reduction. To analyse further, a comparative of σ_{dc}, ν_h and exponent are plotted.

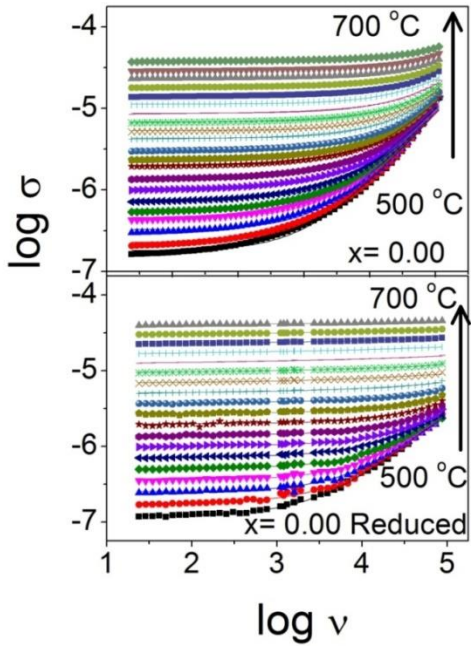

Figure 4.11: Comparative of logσ vs log ν of the fresh and reduced x = 0.0 sample

Figure 4.12 shows the comparative of lnσ vs 1000/T, exponent vs temperature with error bars and log σ_{dc} and log ν_h of the fresh x = -0.01, 0.0 and 0.01 samples and reduced samples x = -0.01, 0.0 and 0.01. It is observed that the conductivity at x = -0.01 is increased, and the value of exponent is reduced reaching nearly sub linear regime after reduction. Moreover, conductivity for x = 0.0 and 0.01 sample is increased in the high temperature regime and reduced in the low-temperature regime after reduction. Simultaneously, activation energy is observed to increase after reduction and crosses 2 eV. The value of exponent for x = 0.0 sample shows an increase at ~ 600 ℃ with a maxima and further decreases after reduction. Simultaneously, in log σ_{dc} and log ν_h, two regimes are formed before and after the kink observed in exponent graph for x = 0.0. These two regimes show sub linear frequency dependence, as mentioned in Fig. 4.12. Further, the value of exponent for x = 0.01 shows a maxima at 600 ℃ before and after reduction and thereafter decreases in reduction. But the

value of exponent is less than 1 before and after reduction as confirmed through log σ_{dc} and log ν_h plots. Hence, there is super linear behaviour in x = - 0.01 sample which approaches unity after reduction. To further analyse, the super linear and sub linear behaviour with composition and reduction, mean free ion life time of charge carriers is evaluated (Fig. 4.13).

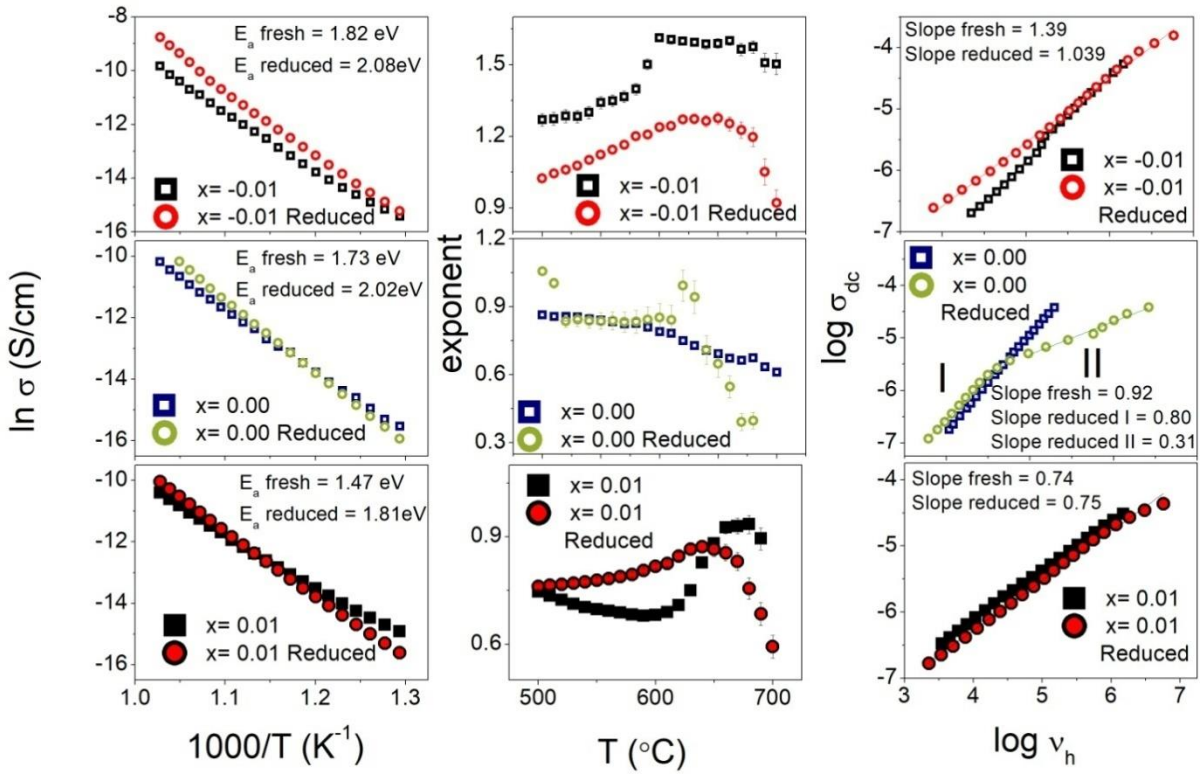

Figure 4.12: Comparative of lnσ vs 1000/T, exponent vs temperature with error bars and log σ_{dc} and log ν_h of the fresh and reduced x = -0.01, 0.0 and 0.01 samples

Figure 4.13 depicts the mean free ion lifetime evaluated on the basis of the probability of the transition rate from the site to vacant site for the reduced and fresh compositions, and inset depicts the linear fitting of log $\nu_h$vs 1000/T to find the characteristic mean free ion life time. The data is well fitted with the model showing χ^2>0.99.

$$\frac{1}{\tau} = \frac{1}{\tau_0}\exp\left(-\frac{E_0}{k_B T}\right) \qquad (4.2)$$

The equation for ionic conductivity is,

$$\sigma = \frac{1}{3}\left(\frac{(Ze)^2}{k_B T}\right) n_i a_0^2 v_0 exp(-E_0/k_B T) \quad (4.3)$$

Using equations 1 and 2,

$$\frac{\sigma}{\nu} = \frac{1}{3}\left(\frac{(Ze)^2}{k_B T}\right) n_i a_0^2 = \alpha n_i \quad (4.4)$$

where n_i is the number density of ionic species, a_0 is the hopping length.

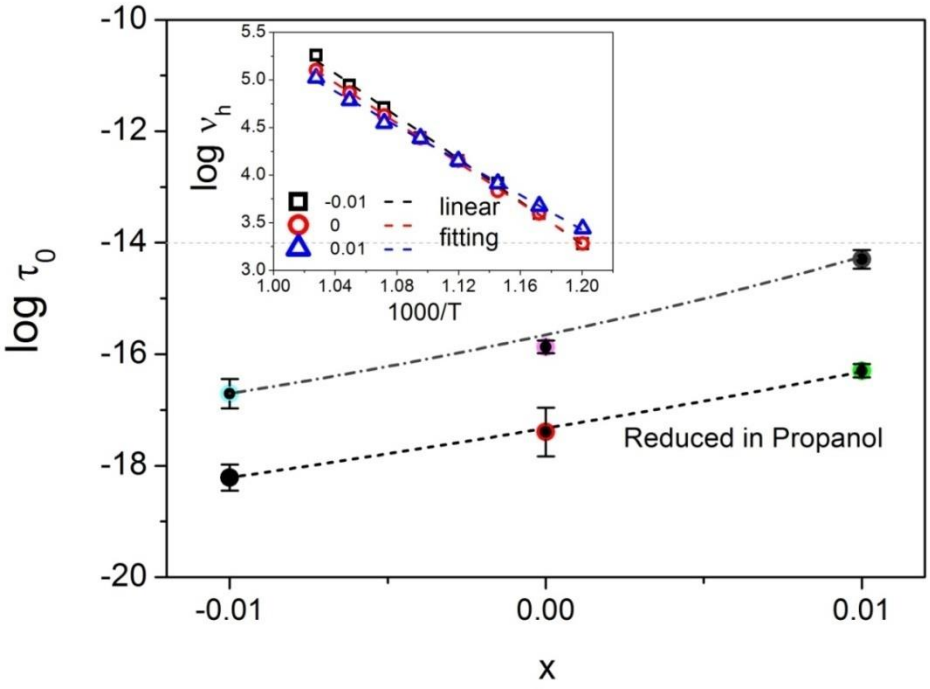

Figure 4.13: Comparative of log τ_o vs x of the fresh and reduced x = -0.01, 0.0 and 0.01 samples, (inset) Linear fitting of log ν_h vs 1000/T of the fresh x = -0.01, 0.0 and 0.01 samples

It is observed that in fresh samples have the mean free life time is in between 10^{-14} s (intramolecular vibration modes) and 10^{-17} s. However, with the reduction, the relaxation time reduces from 10^{-16}s which corresponds to the relaxation due to the electronic species. Hence, x = 0.01 is the ionic composition amongst the others, while x = -0.01 is the electronic composition showing the super linear behaviour due to major electronic contributions. It can

also be observed that with the reduction, the ionic species decreases while the electronic species increases. From equation 4.3, charge carrier concentration can be estimated[182]. The obtained expression is similar to the estimation of ionic charge carrier concentration proposed by Almond and West, i.e., $\sigma_0/\nu_p \approx N$; where σ_0 is a dc conductivity, ν_p hopping frequency and N is effective value mobile ionic charge in coulomb, estimated taking the ratio of dc conductivity and hopping frequency obtained from JPL.

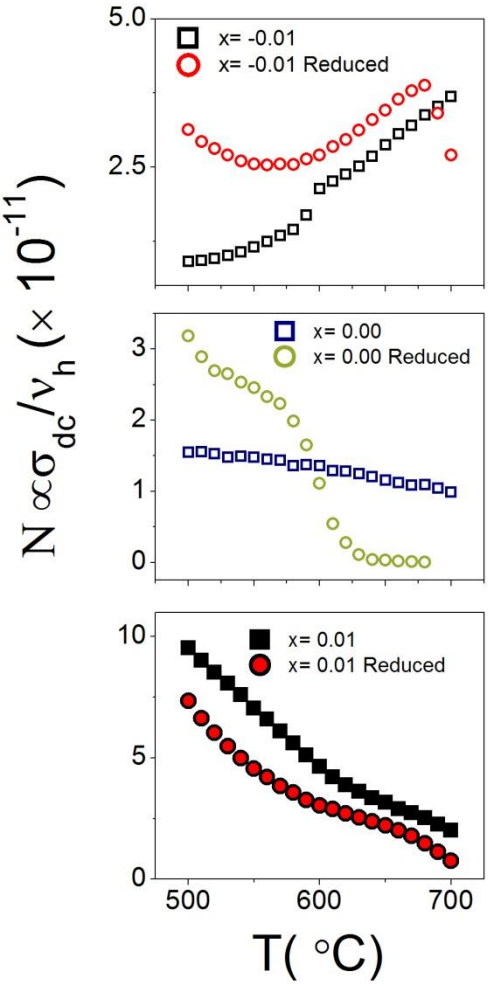

Figure 4.14: Variation of the value of concentration of mobile charge ions with temperatureof the fresh and reduced x = -0.01, 0.0 and 0.01 samples

Figure 4.14 depicts the variation of carrier concentration with temperature. It is observed that the value of N increases with the temperature for x = -0.01 and increases after 600 ℃ in the reduced x = -0.01. For x = 0.0, N is nearly constant with temperature before reduction while it decreases after reduction. Further, for x = 0.01, N reduces with temperature before and after reduction. This shows the existence of predominantly electronic species in the compositions and a mixed ionic–electronic behaviour. Further, the ionic and electronic nature is also predicted through tanδ plots with temperature before and after reduction of the fresh x = -0.01, 0.0 and 0.01 samples (Fig. 4.15).

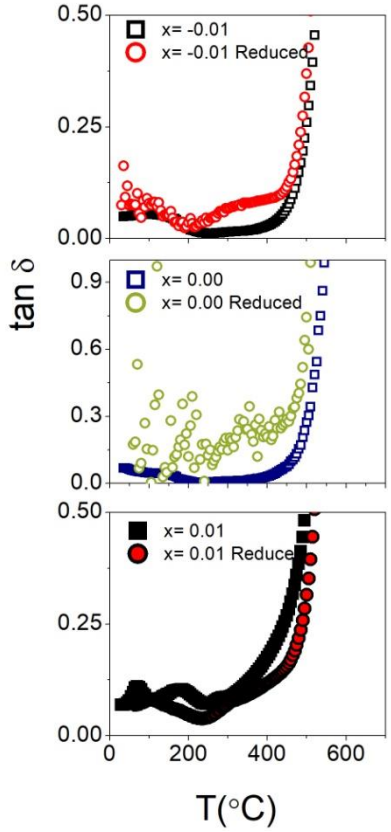

Figure 4.15: Variation of tanδ with temperature of the fresh and reduced x = -0.01, 0.0 and 0.01 samples

It is observed that the value of tan δ rises sharply at 400 ℃ for x =0.0 and -0.01 fresh sample while there is jumbled data in x = 0.0 sample after reduction, but the rise is at 400 ℃

showing Type II behaviour before and after reduction. At x = 0.01, the rise in tanδ is below 400 ℃ in the fresh sample, while in reduced sample, this rise is above 400 ℃ showing the conversion from ionic to the electronic one.

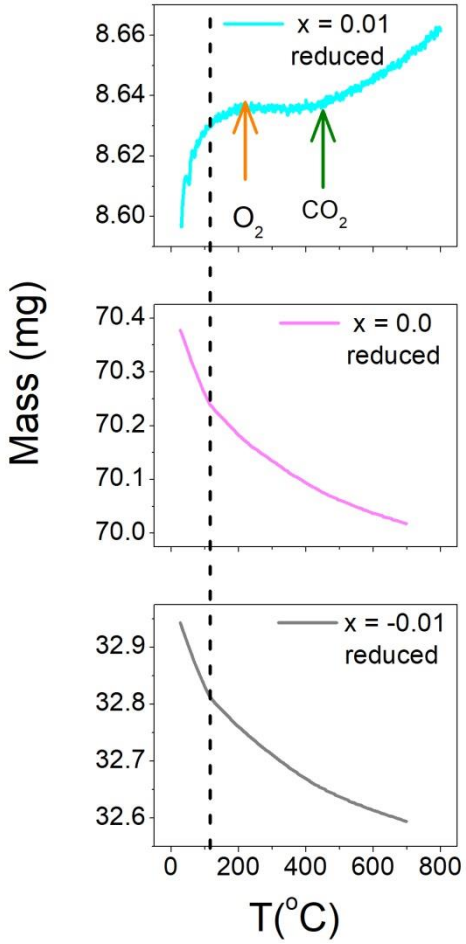

Figure 4.16: Thermogravimetric analysis of the reduced $Na_{0.5+x}Bi_{0.5-x}TiO_{3-\delta}$ (x = -0.01, 0.0 and 0.01) compositions

A gradual mass loss is observed for x = -0.01 sample with a kink at nearly 100 ℃ (shown in Fig. 4.16). For x = 0.0 sample, mass loss with a kink and a change in slope is observed at ~100 ℃, 300 ℃. These kinks correspond to the weight loss due to H_2O and O_2 as the weight loss observed are ~ 2%, 3.5%, respectively. Further, δ has been estimated using the following reaction and observed that the sample has become more oxygen-deficient upon reducing, i.e.

δ = -0.09, -0.08 and 0.01, respectively for x = -0.01, 0.0 and 0.01 in comparison to the δ obtained from TGA before reducing (see Table 4.3).

In order to understand the mechanism, let us summarise the observation from the results obtained so far. For convenience, we are summarizing below in three subgroups as:

Bi rich sample (x = -0.01): The lattice is observed to expand, and conductivity and activation energy are observed to increase after reduction. The super linear frequency dependence decreases to nearly unity after reduction. The mean free ion life time decreases after reduction showing the conversion from mixed ionic electronic to electronic.

Stoichiometric sample (x = 0): The lattice contracts with the increase in conductivity in high-temperature regime after reduction. The conductivity is also observed to reduce in low-temperature regime after reduction. In addition, the activation energy increases after reduction. The sub linear frequency dependence increases to nearly unity after reduction. The mean free ion life time decreases after reduction showing the conversion from mixed ionic electronic to electronic.

Na rich sample (x = -0.01): The lattice contracts with the increase in conductivity in high temperature regime after reduction. The conductivity is also observed to reduce in low temperature regime after reduction. In addition, the activation energy increases after reduction. The sub linear frequency dependence decreases after reduction. The mean free ion life time decreases after reduction.

The activation energy (increases) and mean free ion life time (decreases) show a uniform trend with reduction in all the compositions. In addition, the samples have become more O deficient upon reduction with the alteration in Na^{+}/Bi^{3+} ratio. Thus in the reduced samples, the

transition probability rate of ion hopping reduces which leads to the decrease in ionic conductivity in spite of the increase in O vacancies and coupled electrons after reduction. Additionally, on the basis of observation that the pH of propan-2-ol slightly increased due to the samples and the formation of $C_6H_9BiO_6$ as secondary phase, we can speculate the partial conversion of alcohol to carboxylic acid (C_3H_7OH to C_2H_5COOH). This is also reflected in the structure modification after reduction. This may be coupled to the alterations along c-axis led by the Bi ion lone pair, which is affected through reducing conditions.

4.5 Conclusion

The ion dynamics of the non-stoichiometric $Na_{0.5+x}Bi_{0.5-x}TiO_{3-\delta}$ (x = -0.02, -0.01, 0.00, 0.01, 0.02) is investigated. A very small non-stoichiometry doesn't affect the conductivity but the activation energy is varying in between 1.4 - 1.8 eV, suggesting the variation in charge species. After reduction, the conductivity in Bi rich sample (x = -0.01) enhances and with the increase in Na content, conductivity increases in high temperature regime and reduces in low temperature regime. Further, the increase in activation energy 0.3-0.4 eV in all the samples is coupled with the increase in oxygen vacancies and their coupled electrons. This has led to the alteration in the super linear frequency dependent behaviour to nearly unity suggesting the conductivity is only governed through migration of oxygen ions in x = - 0.01 sample (as of now the sample is O rich after reduction). This is also confirmed through the increase in electronic content from mean free ion life time and the loss tangent behaviour.